Heat Transfer and Phase Change in Deep CO_2 Injector for CO_2 Geological Storage

Kyuro Sasaki and Yuichi Sugai
Department of Earth Resource Engineering, Kyushu University
Japan

1. Introduction

CO_2 capture and storage (CCS) is expected to reduce CO_2 emissions into the atmosphere. Various underground reservoirs and layers exist where CO_2 may be stored such as aquifers, depleted oil and gas reservoirs as well as unmined coal seams.

Coal seams are feasible for CCS because coal can adsorb CO_2 gas with roughly twice volume compared with CH_4 gas originaly stored (Yee et al., 1993). However, the coal matrix is swelling with adsorbing CO_2 and its permeability is reduced. Supercritical CO_2 has a higher injection rate of CO_2 into coal seams than liquid CO_2 because its viscosity is 40% lower than the liquid CO_2 (see Harpalani and Chen, 1993).

The Japanese consortium carried out the test project on Enhanced Coal Bed Methane Recovery by CO_2 injection (CO_2–ECBMR) at Yubari City, Hokkaido, Japan during 2004 to 2007 [Yamaguchi et al. (2007), Fujioka et al.(2010)]. The target coal seam at Yubari was located about 890 to 900 m below the surface (Yasunami et al., 2010). However, liquid CO_2 was injected from the bottom holes because of heat loss along the deep injection tubing. The absolute pressure and temperature at the bottom hole was approximately 15.5MPa and 28°C. The regular tubing was replaced with thermally insulated tubing that included an argon gas layer but the temperature at the bottom was still lower than the critical temperature of CO_2.

This chapter provides a numerical model of heat transfer and calculation procedure for the prediction of CO_2 temperature and pressure that includes a phase change (supercritical or liquid) by considering the heat loss from the injector to surrounding casing pipes and rock formation. Furthermore, this study provides numerical simulation results of the temperature distribution of the coal seam after the injection of CO_2.

2. Prediction model for CO_2 injection temperature

2.1 CO_2 flow rate injected into a reservoir

As shown in Fig. 1, a schematic radial flow model in a reservoir, such as coal seam or aquifer, is targeted for CO_2 injection with vertical injection well (injector). The reservoir with radius R and thickness h_R, is saturated with water and open with constant pressure at its outer boundary. Assume omitting well pressure loss, the initial CO_2 mass flow rate , $M(0)$, at time t = 0, that is injected into the reservoir from its bottom hole, is equal to radial water flow rate in the reservoir [Michael et al. (2008) and Sasaki & Akibayashi (1999)],

$$M(0) = \rho_{BH} \frac{P_{BH}(0) - P_R}{\dfrac{\mu_w}{2\pi K_w h_R} \cdot \ln\left(\dfrac{R}{r_w}\right)} \quad ; \quad P_{BH}(0) = P_{WH}(0) + g\int_0^H \rho(x,0)\ dx \tag{1}$$

where $\rho(x,t)$ and $\rho_{BH} = \rho(H,t)$ are CO_2 density in the injector and bottom hole respectively, g is acceleration of gravity, r_w is outer radius of the bottom hole, K_w is reservoir permeability, P_{WH}, P_{BH} and P_R are pressures at well head, bottom hole and injector outer boundary, μ_w is water viscosity in the reservoir, and H is length of vertical injector. The reservoir initial pressure is also equal to P_R.
After starting CO_2 injection, the CO_2 mass flow rate $M(t)$ and bottom hole pressure $P_{BH}(t)$ are changing with elapsed time t, since bottom hole pressure depends on CO_2 density distribution through the injector and water is replaced with CO_2. Therefore, flow rate after becoming steady-state Q is given with P_{BH} and CO_2 viscosity μ_f at $t = \infty$.

$$M(\infty) = \rho_{BH}(\infty) \frac{P_{BH}(\infty) - P_R}{\dfrac{\mu_f}{2\pi K_w h_R} \cdot \ln\left(\dfrac{R}{r_w}\right)} \quad ; \quad P_{BH}(\infty) = P_{WH}(\infty) + g\int_0^H \rho(x,\infty)\ dx \tag{2}$$

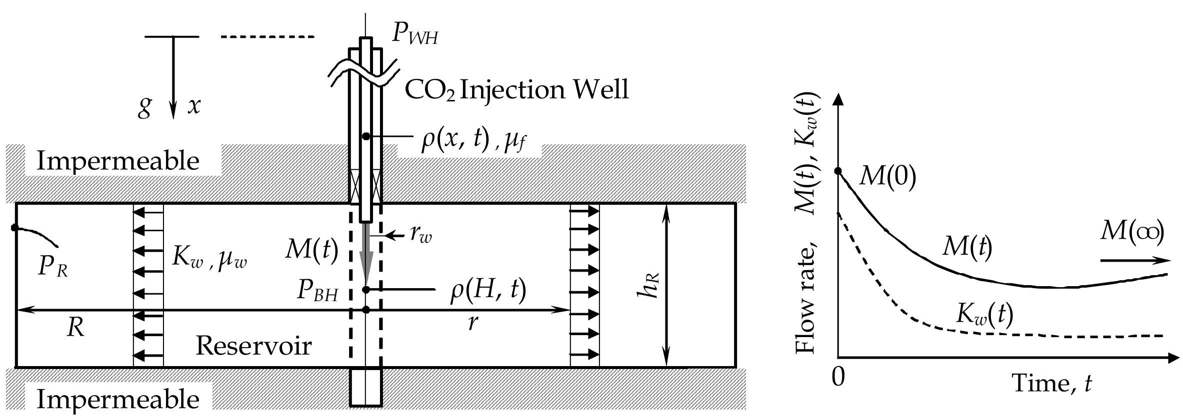

Fig. 1. Schematic radial flow model for injected CO_2 into a reservoir filled with water

Generally, CO_2 viscosity (30°C, 15MPa) is much smaller than water (roughly 1/30), thus the flow rate increases with t. Furthermore, viscosity of supercritical CO_2 is smaller than liquid CO_2. On the other hand, the flow rate Q strongly depends on reservoir permeability times height (=$K_w h_R$). Especially coal seams have relatively low permeability of order 10^{-15} m^2. It has been reported by some projects that permeability of coal seams decreased with rough ratio of 1/10 to 1/100 after CO_2 injection due to swelling of coal matrix by CO_2 adsorption [Clarkson et al. (2008) and Sasaki et al. (2009)].

2.2 Unsteady heat conduction equation

Figure 2 shows schematic diagram of radial heat loss from a vertical injection well (injector) that is consisting tubing pipe, casing pipes and well annulus. CO_2 is flowed down through the tubing pipe, and injected from bottom of the well with perforated holes. The annulus between two coaxial pipes is not used for CO_2 injection, and possibly needed to prevent heat loss from the tubing.

In present analytical approaches, inside area of the casing pipe is assumed as quasi-steady and outer region of the casing pipe ($r \geq r_{cao}$) is analyzed by unsteady equation of heat conduction. For the outer cement and rock region at a level, Fourier's second law in cylindrical coordinates (r, x) is expressed as;

$$\frac{\partial\theta}{\partial t} = a_r\left(\frac{\partial^2\theta}{\partial r^2} + \frac{1}{r}\frac{\partial\theta}{\partial r} + \frac{\partial^2\theta}{\partial x^2}\right) \cong a_r\left(\frac{\partial^2\theta}{\partial r^2} + \frac{1}{r}\frac{\partial\theta}{\partial r}\right) \tag{3}$$

where θ (°C) is rock temperature, t(s) is elapsed time, r(m) is radius, a_r(m²/s) is the heat diffusivity of rock. Heat conduction in vertical direction, x, can be omitted by comparing with that of radial direction. Analytical solution has been presented by Starfield & Bleloch (1983) for unsteady-state rock temperature distribution around underground airways. Especially, they presented a method to simulate internal surface temperature using with Biot number and elapsed time factor function of Fourier number (see section 2.7).

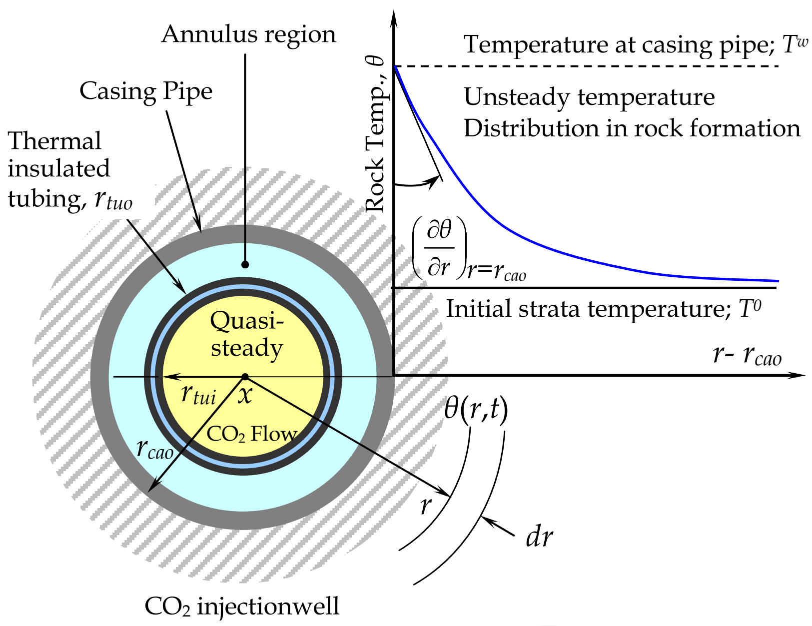

Fig. 2. Schematic diagram of radial heat flow from a vertical injection well (cross section)

2.3 Four thermal phenomena considered along CO_2 injection well

Figure 3 shows a schematic of heat transfer phenomena at an injection well. Four thermal phenomena were considered for the construction of the numerical model that is used for predicting CO_2 temperature and pressure at the bottom hole.

1. Natural convection in the annulus, filled with N_2 or water, increases heat transfer from tubing to casing, cement and rock formation. The heat transfer coefficient or Nusselt number at a specific depth is determined by using a formula reported by Choukairy et al. (2004).
2. The thermal performance of insulated tubing containing an argon shield layer was evaluated by considering the vertical convection flow of argon, thermal radiation between inner surfaces of the argon layer and thermal conduction at the tubing joints. Thermal characteristics of the insulated tubing are able to be corrected against the

original heat conductivity of argon gas using a number n determined by a field test and also by well logging data (see section 2.5).
3. The CO_2 phase was determined by its specific enthalpy which can be calculated from the pressure, temperature and heat loss along the well.
4. An unsteady analytical solution of the outer-surface temperature of casing pipe, expressed with Eq.(1), can be applied against the elapsed time from the start of CO_2 injection.

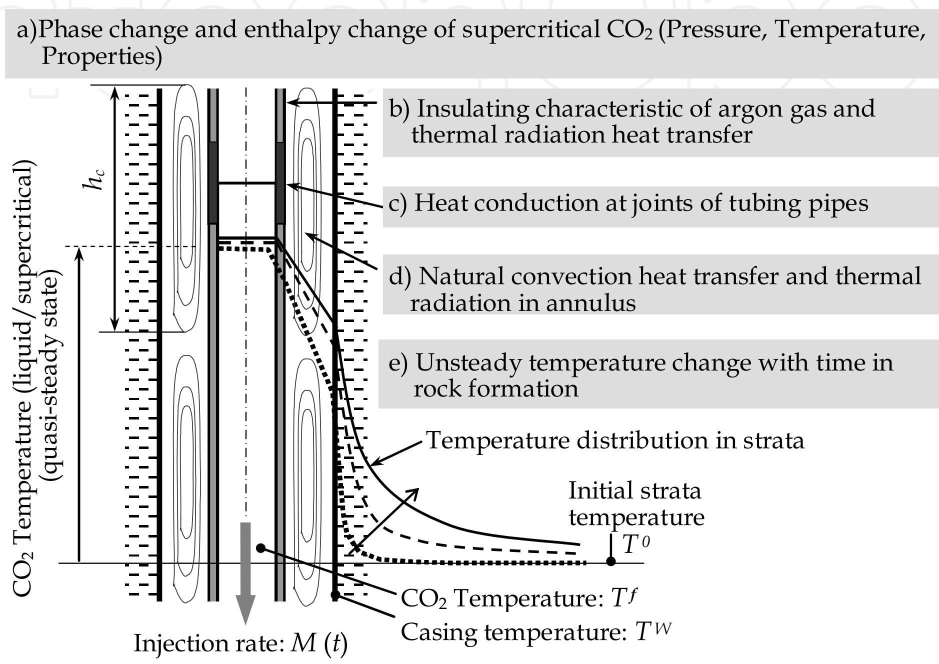

Fig. 3. Heat transfer phenomena from fluid flow in injector to surrounding rock formation

2.4 Overall thermal conductivity of the quasi-steady state region of the injection well

Figure 4 shows an example of the well structure (Yubari CO_2-ECBMR pilot-test site). CO_2 heat loss occurs during flow down to the bottom and propagates through various cylindrical combinations of steels and fluids with various thermal properties in the well configuration. To evaluate heat loss the overall heat conductivity that consists of conductivities of well materials and convective heat transfer rates of fluid flows that are contained in the well are important. Equations (4) and (5) represent single tubing and thermally insulated tubing, respectively (Nag, 2006).

$$\lambda = \frac{1}{\dfrac{\ln\dfrac{r_{cao}}{r_{cai}}}{\lambda_{Steal}} + \dfrac{\ln\dfrac{r_{cai}}{r_{ruo}}}{N_u \cdot \lambda_f} + \dfrac{\ln\dfrac{r_{tuo}}{r_{tui}}}{\lambda_{Steal}} + \dfrac{1}{r_{tui}\alpha_i}} \tag{4}$$

$$\lambda = \frac{1}{\dfrac{\ln\dfrac{r_{cao}}{r_{cai}}}{\lambda_{Steal}} + \dfrac{\ln\dfrac{r_{cai}}{r_{thco}}}{N_u \cdot \lambda_f} + \dfrac{\ln\dfrac{r_{thco}}{r_{thci}}}{\lambda_{Steal}} + \dfrac{\ln\dfrac{r_{thci}}{r_{tho}}}{n \cdot \lambda_{Ar}} + \dfrac{\ln\dfrac{r_{tho}}{r_{thi}}}{\lambda_{Steal}} + \dfrac{1}{r_{thi}\alpha_{thi}}} \tag{5}$$

Where α_{thi} is the heat transfer coefficient at the inner wall of the tubing pipe, λ_f is the heat conductivity of the fluid (water) in the annulus, λ_{Steal} is the heat conductivity of the casing and tubing pipes, N_u ($=\alpha_f \cdot r_{thco}/\lambda_f$) is the Nusselt number for the annulus and n is a correction number to adjust the heat conductivity of the argon gas layer in the insulated tubing.

2.5 Evaluation of performance of thermal insulated tubing

Thermal insulated tubing pipe is sometime used for geo-thermal wells through cold formation in order to prevent heat loss from produced hot spring water/steam. In case of the Yubari injected CO_2-ECBMR test, connected thermal insulated tubing pipes 20 m in length were used partially in 2005-2006 and totally in 2007. The insulated tubing includes argon gas shield layer is enclosed between inner and outer pipes to prevent heat loss from inside ideally with low thermal conductivity of argon gas; 0.116 W/m°C. However, joints between pipes are not shielded, and natural gas convection flow in the shield is expected to make increase the heat loss trasfered from the flow to outer tubing.

Fig. 4. Test to evaluate of equivalent thermal conductivity in the thermal insulated tubing using by pulsed heating carried at Yubari CO_2-ECBMR test field (Oct. 10, 2006) (see Yasunami et al., 2010)

To evaluate the thermal performance of the insulated tubing, tests using a insulated tubing pipe were carried out by pulsed heating from inside and measurements of outer and inner surface temperatures of the pipe placed horizontally as shown Fig. 4. Furthermore, the equivalent thermal conductivity was analyzed with Choukairy et al.'s equation (see section 2.5) and the history matching study for the well logging data. The thermal conductivity correction factor for conductivity of argon gas, n, is evaluated as shown in Fig. 5.

The equivalent heat conductivity including inside convective heat transfer was evaluated as three times larger as that of original argon gas without longitudinal heat loss through to connected tubing pipes. The correction factor, n, was introduced to adjust the equivalent heat conductivity of the tubing based on the original heat conductivity of argon gas. It was determined to be n = 3 but heat loss through the joints that are between the insulated tubing was not included in the test. The thermal equivalent conductivity of the insulated tubing was determined to be n = 4 or λ = 0.21W/m°C based on the well logging temperature at the Yubari CO_2-ECBMR test site and the measurement data were obtained from the heater response test carried out in the test field.

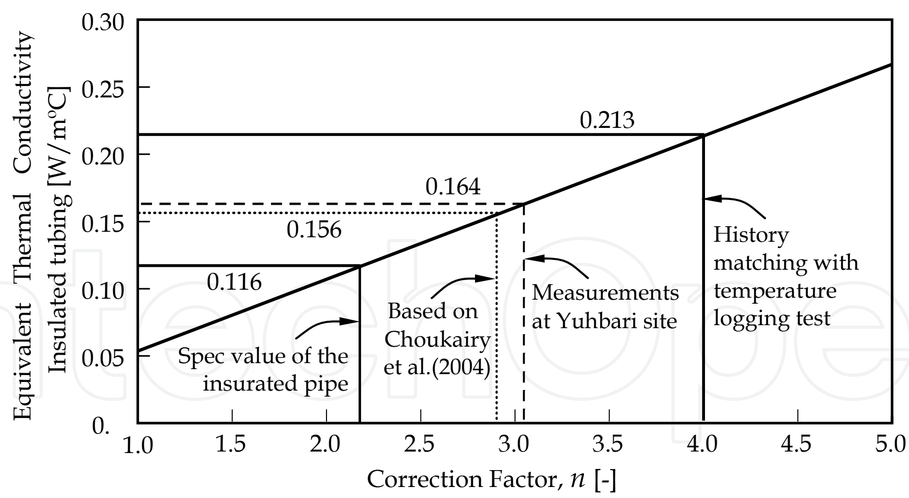

Fig. 5. Thermal conductivity correction factor for shielding with argon gas (*; spec value provided by a steel pipe maker)

2.6 Convective heat transfer in the annulus

Natural convection of annulus fluids makes influences on the heat transfer rate from the tubing pipe to the surrounding casing pipe and the formation. Choukairy et al. (2004) presented the following formula for the Nusselt number, N_u, for natural convection flow in an annulus with various radius ratios:

$$N_u = \frac{\alpha_f L}{\lambda_f} = \frac{\kappa}{mA}(P_r R_a)^{1/4} \cdot T_m^{\ 5/4} \tag{6}$$

where α_f denotes the natural convection heat transfer coefficient on the inner surface of the casing, L (=r_{cai} - r_{tuo}) is the width of the annulus, κ is the radius ratio, m is a constant defined by Choukairy et al., A is the aspect ratio, P_r is the Prandtl number, Ra is the Rayleigh number and T_m is a dimensionless temperature defined by following equations:

$$A = \frac{h}{L} \tag{7}$$

$$\kappa = \frac{r_{cai}}{r_{tuo}} \tag{8}$$

$$R_a = \frac{g\beta_T (T^f - T^w) \cdot h_c^{\ 3}}{a_f \cdot \upsilon_f} \tag{9}$$

$$T_m = \frac{1}{1-\kappa^{4/5}} \tag{10}$$

where h_c is the circulation height of natural convection flow, g is the acceleration of gravity, β_T is the coefficient of thermal expansion of the fluid, υ_f is the dynamic viscosity and a_f is heat diffusivity of fluid in the annulus. The Nusselt number, N_u, calculated by Eq.(4) was used for each elevation.

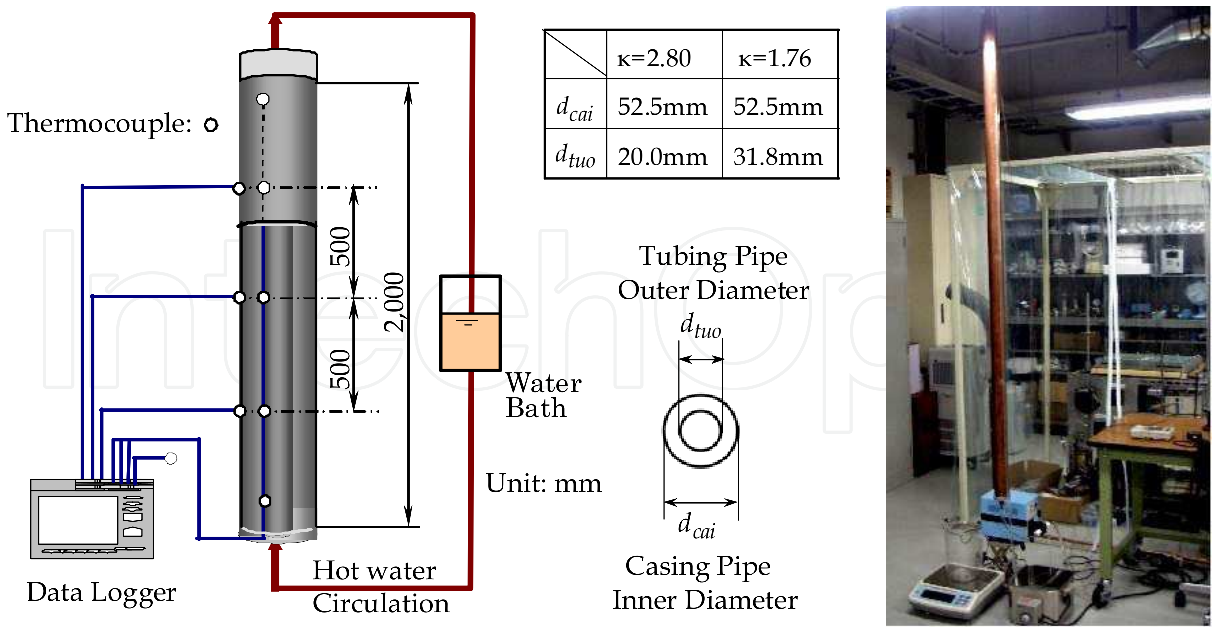

Fig. 6. Experimental setup to verify natural convection heat transfer coefficient in the annulus (Yasunami et al., 2010)

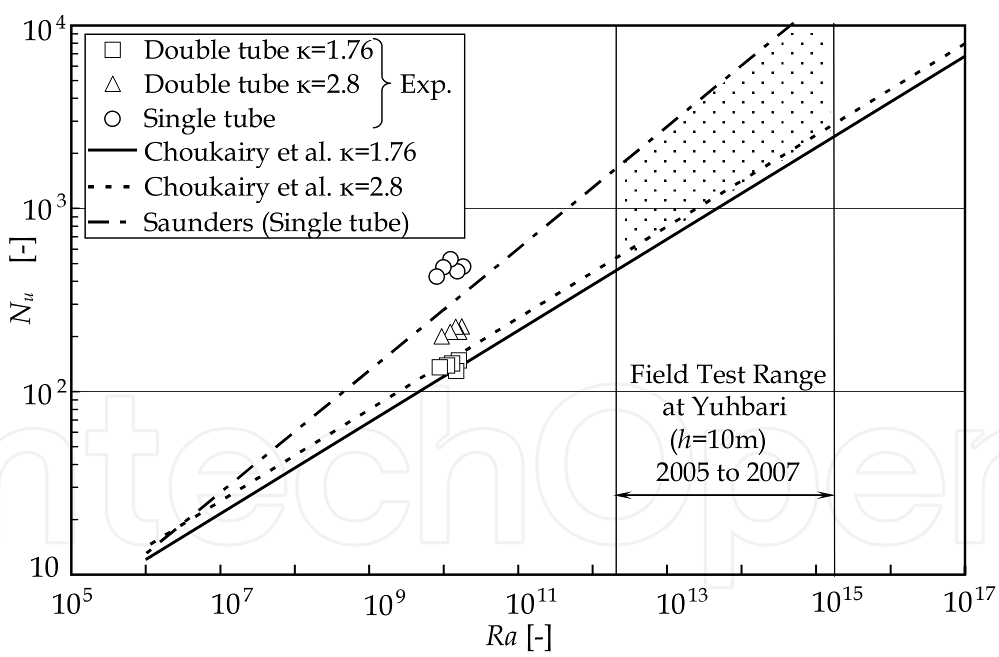

Fig. 7. Experimental results of Nusselt number for convective heat transfer in annulus (Yasunami et al., 2010)

Laboratory experiments were carried out to verify the reliability of Choukairy's equation and to investigate the heat transfer rate using the well models consisting of two copper pipes with different diameters as shown in Fig. 6. Hot water at 40 to 60 °C was circulated through the inner pipe instead of CO_2. Pipe temperatures were measured by T-thermocouples that were placed on the pipe surfaces. Figure 7 shows experimental results obtained for N_u and compared with those from Choukairy's equation. In addition, measured values of N_u on the outer surface of the single tubing determined using the equation proposed by Saunders [after Rohsenow et al. (1998)] were also compared in Fig. 7. Based on these results, we have found that Choukairy's equation is able to evaluate the heat transfer rate in the annulus.

2.7 Unsteady casing temperature

On the other hand, the temperature of the formation outside the casing pipe (outer surface) increases gradually after the injection. Assume T^0 is the initial strata formation temperature and T^{an} is the temperature in the annulus, the temperature at outer surface of the casing T^w, can be given by the solution for the unsteady heat conduction equation; Eq. (3). It has been presented by Starfield and Bleloch (1983):

$$T^{w} = T^{an} + \frac{\eta_t}{\eta_t + B_i}(T^{0} - T^{an}) \tag{11}$$

where η_t is defined as the elapsed time factor and B_i is the non-dimensional Biot number, and B_i is defined by following equation:

$$B_i = \frac{\alpha_{ca} \cdot r_{cao}}{\lambda_r} \tag{12}$$

where α_{ca} is the apparent heat transfer rate at the inner casing and λ_r is the heat conductivity of rock. Starfield and Bleloch (1983) reported equations for the elapsed time factor η_t, which is a function of the Fourier number, τ, and Sasaki & Dindiwe (2002) revised it for $\tau \leq 1.5$ as:

$$\tau \leqq 1.5 \quad ; \quad \eta_t = \frac{1}{[0.9879 + 0.3281(\ln\tau) + 0.03064(\ln\tau)^2} \tag{13}$$

$$1.5 \leqq \tau \leqq 10 \quad ; \quad \eta_t = \frac{1}{[0.979813 + 0.383760(\ln\tau)} \tag{14}$$

$$10 \leqq \tau \leqq 100 \quad ; \quad \eta_t = \frac{1}{[0.839337 + 0.444718(\ln\tau)} \tag{15}$$

$$1000 \leqq \tau \quad ; \quad \eta_t = \frac{2\Lambda(1 - \Lambda - \Lambda^2 - \Lambda^3)}{0.57722} \tag{16}$$

$$\Lambda = \frac{0.57722}{[\ln(4\tau) - 1.15444)} \tag{17}$$

$$\tau = \frac{a_r t}{r_{cao}{}^2} \tag{18}$$

The elapsed time factor η_t vs. Fourier number τ calculated by equations (13) to (18), is presented in Fig. 8.

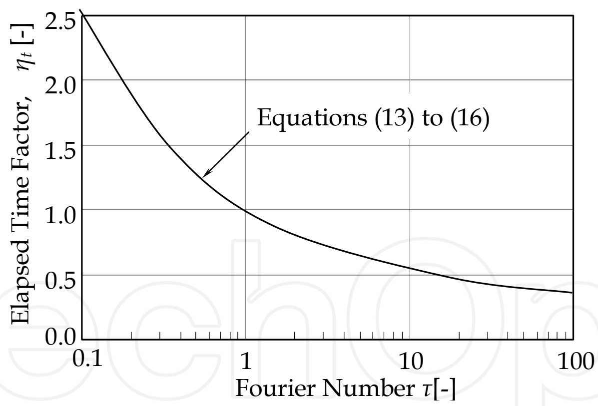

Fig. 8. Elapsed time factor vs. Fourier number

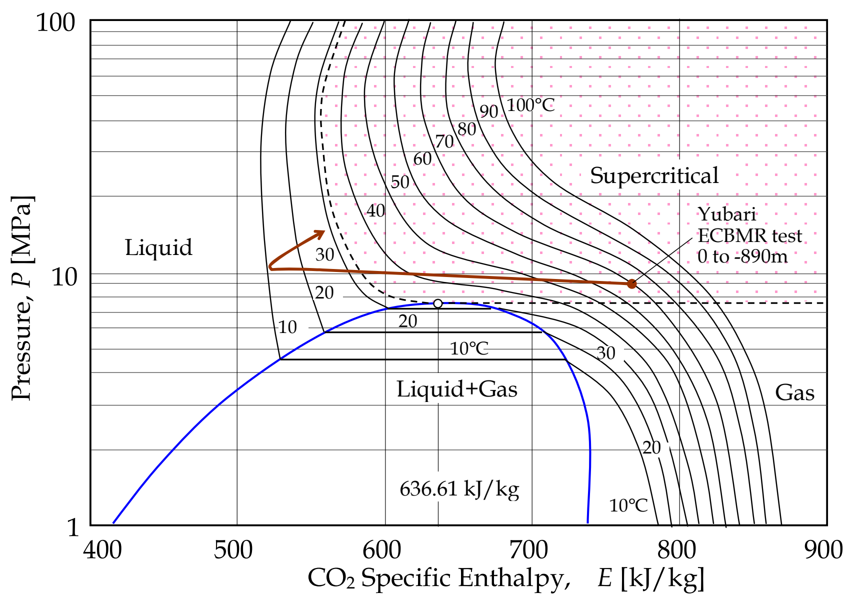

Fig. 9. CO_2 pressure-specific enthalpy and phase diagram calculated with PROPATH(2008) for 10 to 100 °C and 1 to 100 MPa (○; Critical point; 31.1°C and 7.38MPa)

2.8 Numerical equations for the determination of the CO_2 specific enthalpy

Changes in CO_2 temperature and phase (gas, liquid and supercritical) are accompanied by a specific enthalpy change. CO_2 specific enthalpy, $E(P,T)$ may be expressed by:

$$E(P,T) = \int_{T_0}^{T} C_p dT^f + \int_{P_0}^{P} V(1-T_i\beta)dP \tag{19}$$

where V is the specific volume, β is the coefficient of thermal expansion, T_0 and P_0 are triple point temperature (=-56.57°C) and pressure (=0.5185MPa). The diagram CO_2 pressure-specific enthalpy for temperature range 10 to 100 °C and pressure range 1 to 100 MPa, that is calculated by PROPATH(2008), is shown in Fig. 9.

The specific enthalpy of CO_2 decreases with depth x by heat loss from CO_2 flow to the formation around the injection well.

$$\Delta q = 2\pi\lambda(T^w - T^f)\Delta x \tag{20}$$

where T_f is the CO_2 temperature in the tubing, Δx is the length of the element and T_w is the temperature at the outer surface of the casing.

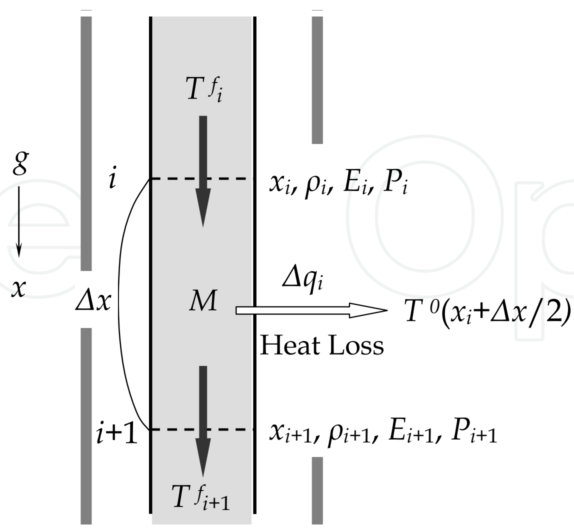

Fig. 10. The numerical calculation model for CO_2 temperature and pressure in the injector

CO_2 temperature T^f_i was calculated using the function shown in Fig. 10. The function used to calculate the temperature T^f_i from the specific enthalpy E_i and pressure P_i is defined as:

$$T_i^f = \theta(E_i, P_i) \tag{21}$$

The heat flow rate, Δq_i, of a small element in the well, Δx_i, may be written as:

$$\Delta q_i = 2\pi\lambda_i (T_i^f - T_i^w)\Delta x_i \tag{22}$$

where λ_i is the equivalent heat conductivity at x_i, T_i^f is the temperature of CO_2 in the tubing and T_i^w is the temperature of the casing outer surface at each element denoted i . The heat generation by flow friction with internal surface of the tubing can be omitted due to very small pipe friction factor and low fluid viscosity for CO_2 flow.

The specific enthalpy of CO_2, E_{i+1} at $x_{i+1}=x_i+\Delta x_i$ is obtained from:

$$E_{i+1} = E_i + \frac{\Delta W - \Delta q_i}{M} \tag{23}$$

where M is the mass flow rate of CO_2 and ΔW is heat generated by a heater during x_i to x_{i+1}.

Using the function $\rho(P_i, T_i)$, calculation of the CO_2 density from P_i and T_i and the CO_2 pressure at x_{i+1}, P_{i+1} is given by;

$$P_{i+1} = P_i + \rho(P_i, T_i)\left(g - f\frac{v^2}{4r_{tui}}\right)\Delta x_i \tag{24}$$

where f and v are friction factor and average velocity of tubing pipe. Then the temperature of CO_2 at x_{i+1} can be obtained from:

$$T_{i+1}^f = \theta(E_{i+1}, P_{i+1}) \tag{25}$$

In these numerical simulations, $E(P,T)$, $\theta(P,T)$ and $\rho(P,T)$ and other fluids properties are calculated using a corresponding software sub-routines, such as PROPATH(Propath Group, 2008) and NIST (2007). Calculation step Δx_i = 1.0m can be used to get enough accuracy (Yasunami et al., 2010).

2.9 Required values in the numerical calculations

For these numerical calculations, three values for each depth are required.

1. Heat diffusivity of formation.
   In Yubari ECBMR test project introduced in this book, no rock core drilling was carried out from o m to -800 m, thus we had to estimate rock properties (Fujioka et al., 2010). The heat conductivity λ_r and the heat diffusivity a_f of the rock formation outer casing have not been measured previously, so values of a_r=1.30×10^{-6} m^2/s and λ_r=1.30 W/mK were assumed and this was based on standard heat properties of sedimentary rocks (Yasunami et al., 2010).
2. Circulation height of natural convection flow in the annulus.
   It was difficult to measure the circulation height h of natural convection in the annulus at the Yubari site. However, the bottom hole temperature was not sensitive to h, even when h changed from 5 to 20 m. Thus h =10m was assumed as an appropriate value since natural convection was not observed at lower than 2m in the experiments described in the previous section.
3. Heat capacity of the tubing or casing.
   We assumed that temperature changes of tubing and casing pipes were quasi-steady and thus the heat capacity of these pipes was not included in the equations.

3. Results of Yubari ECBMR test project

3.1 Injection well formation

Figure 11 shows a well structure and formation used at the Yubari CO_2-ECBMR test project in 2005. CO_2 heat loss occurs during flow down to the bottom and propagates through various cylindrical combinations of steels and fluids with various thermal properties in the well configuration. Table 1 shows conditions used for the models from 2005 to 2007 carried out in the project denoted as;

a. Model 2005:
   The well was drilled in 2005 (hereafter denoted as Model 2005) and consisted of thermally insulated tubing 180 m in length from the well head.
b. Model 2006:
   In 2006, thermally insulated tubing of 180m in length was used at the head (0 to 180m) and the bottom (650 to 890m) while the annulus was filled with liquid CO_2.
c. Model 2007:
   In 2007 all the injection pipe tubing was replaced with thermally insulated tubing of 890 m in length and H_2O was used to fill the annulus. This was done to minimize heat loss from the tubing and thus keep CO_2 in its supercritical condition.
d. Heater Model 2007:
   To overcome the difficulty of low temperature and low injection rate, numerical predictions were done considering the use of an electric line heater to heat up CO_2 flow at the position of 180m from the surface. The heater capacity of W = 1.43kW was chosen because of the cable strength and restrictions of materials against corrosion of supercritical CO_2.

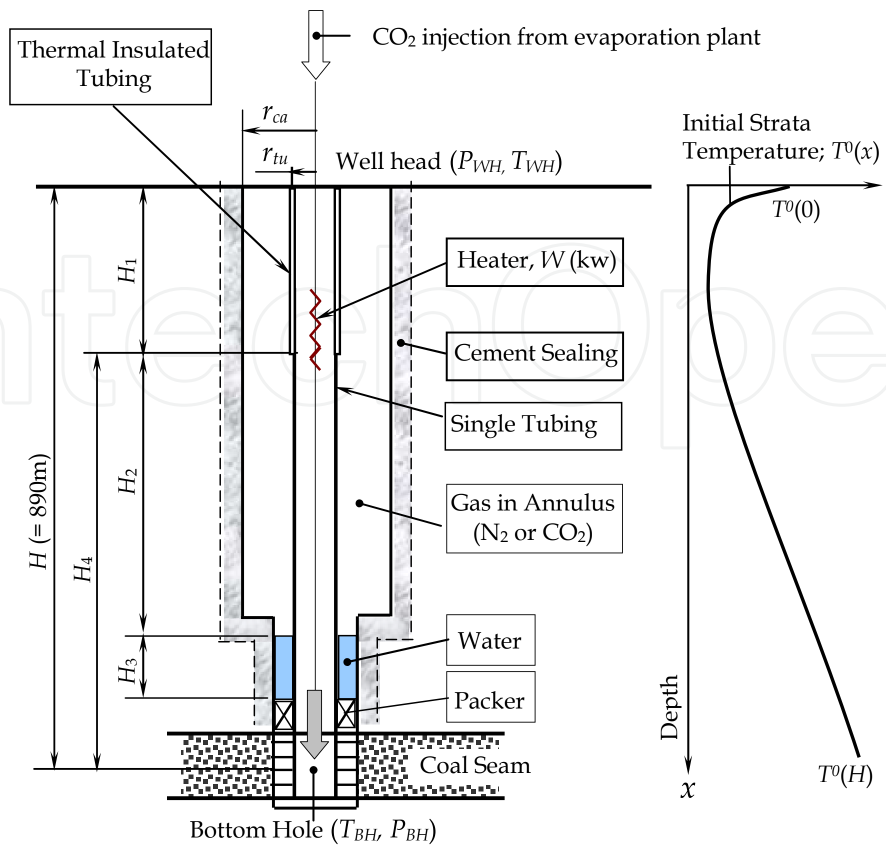

Fig. 11. An example of CO_2 injection well formation, initial strata temperature and schematic annulus formation (Yubari CO_2-ECBMR test project, Model 2005)

Term/Model		Model 2005	Model 2006	Model 2007	Model 2007+ Heater
Temp. and Press. At well head (T_{WH}, P_{WH})		70 °C 9.0 MPa	70 °C 9.0 MPa	70 °C 8.6 MPa	70 °C 8.6 MPa
S. Enthalpy at well head; E_{WH}(kJ/kg)		766.34	766.34	771.27	771.27
Injection rate M(kg/day)		3000	3000	3000	11000
Tubing	H_1; x=0~180m	Insulated tube	Insulated tube	Insulated tube	Insulated Tube
	H_2; x=180~667m	Single tube	Single tube	Insulated tube	Insulated Tube
	H_3; x=690~890m	Single tube	Insulated tube	Insulated tube	Insulated Tube
Fluid in annulus	for H_1	N_2 Gas	Liquid CO_2	Water	Water
	for H_2	N_2 Gas	Liquid CO_2	Water	Water
	for H_3	Water	Water	Water	Water
Heater output; W(kW) (x=0~255m)		0	0	0	1,430

Table 1. Parameters of injection well formation for CO_2 injection

3.2 Effect of natural convection in the annulus

The results of temperature prediction against depth after one day by the heat conduction model (N_u=1 and n=1) and the heat convection model for an injection temperature of 70°C, an injection pressure of 9MPa and an injection rate of 3.0ton/day is shown in Fig. 12.

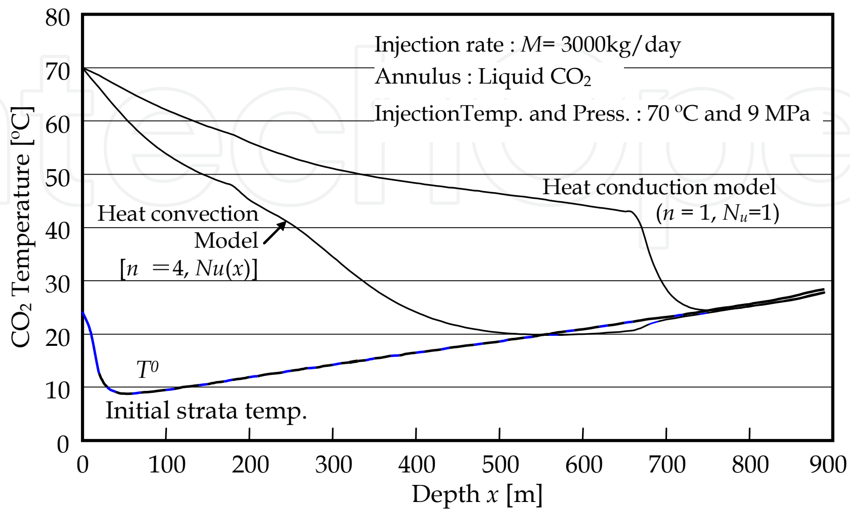

Fig. 12. A comparison of CO_2 temperatures after 1 day between heat conduction and heat convection models (Model 2005, 180m insulated tubing was partly used from well head)

Figure 13 shows comparisons of CO_2 temperature and pressure at the bottom hole. Numerical simulation results for the data, obtained in 2005 at the Yubari field, show that the heat convection model is better than the conduction model. This is because the temperature of the CO_2 decreased by heat loss caused by natural convection in the annulus. The bottom pressure increased because of the increase in CO_2 density that resulted from the CO_2 supercritical to liquid phase change.

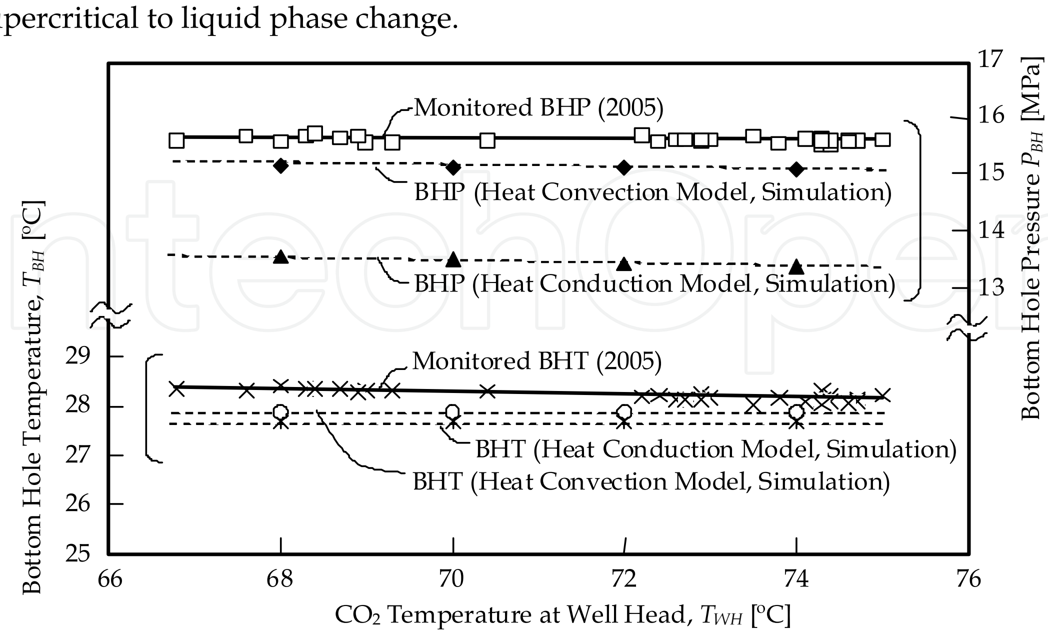

Fig. 13. Comparisons of bottom hole temperature and pressure (BHT and BHP) that were simulated by heat conduction and heat convection models with monitored values (Model 2005)

Figures 14 and 15 show comparisons of CO_2 temperature and pressure between simulations and the well logging data for injection conditions of 68.54°C, 9MPa and 4.5ton/day at the well head. Since logging from the surface to a level of -890m took 2.4hours (Prensky,1992), simulated CO_2 temperatures against depth were plotted for each time segment. The reason for the rise in the measured pressure near the well head of about of 0.3 MPa is unknown at present.

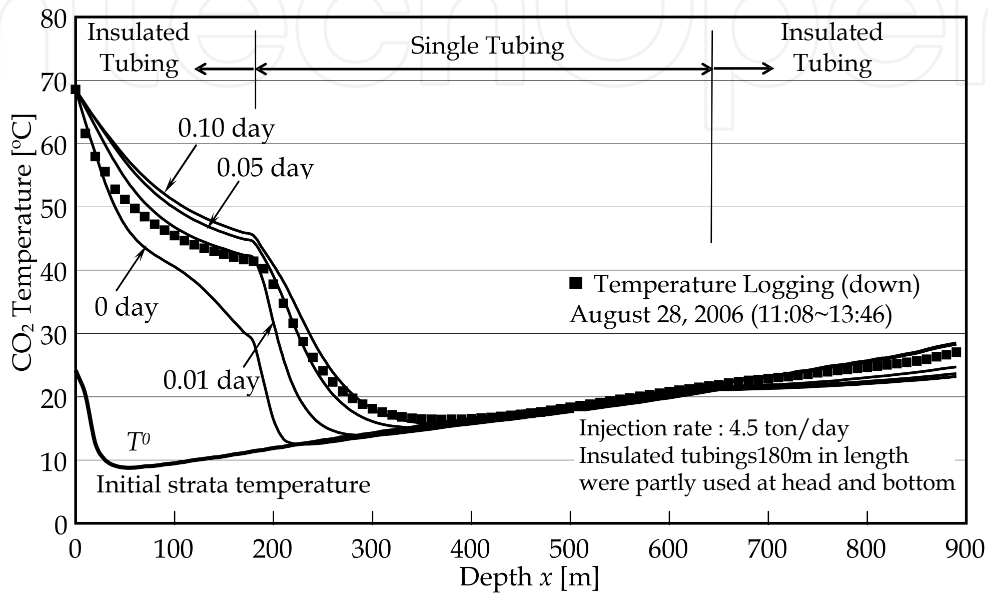

Fig. 14. Comparison between logged temperature and simulation results for Model 2006 (Logging data was obtained on August 28, 2006 (11:08 to 13:46) at the Yubari ECBMR test site)

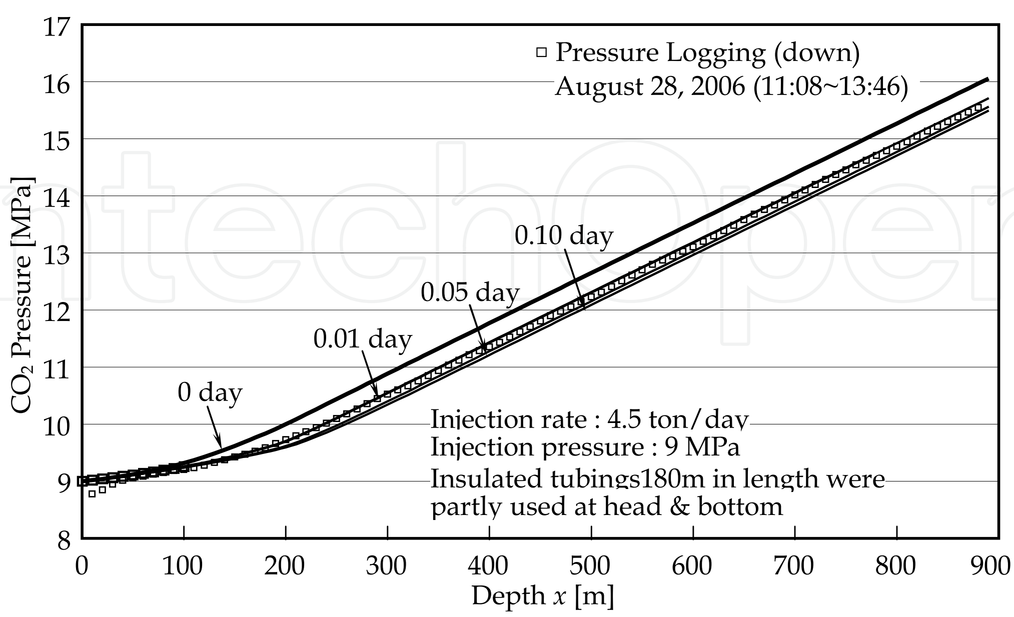

Fig. 15. Comparison between logged pressure and simulation results (Model 2006) (Logging data was obtained on August 28,2006 (11:08 to 13:46) at the Yubari test site).

3.3 Thermal insulated tubing partly used at the well head and bottom (Model 2006)

For the case of Model 2006 of Yubari ECBMR test, numerical simulations at 0, 22 and 68 days are shown in Figure 16. Figures 17 and 18 show the Nusselt number, the heat conductivity, the density and the specific enthalpy versus depth after 1 day.

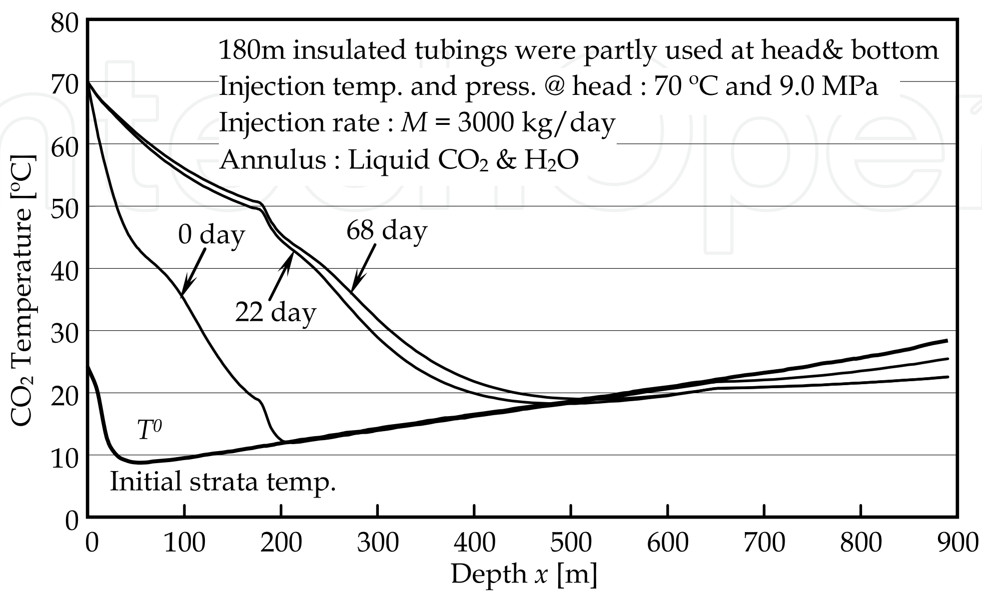

Fig. 16. CO_2 temperature distribution vs. depth (Model 2006).

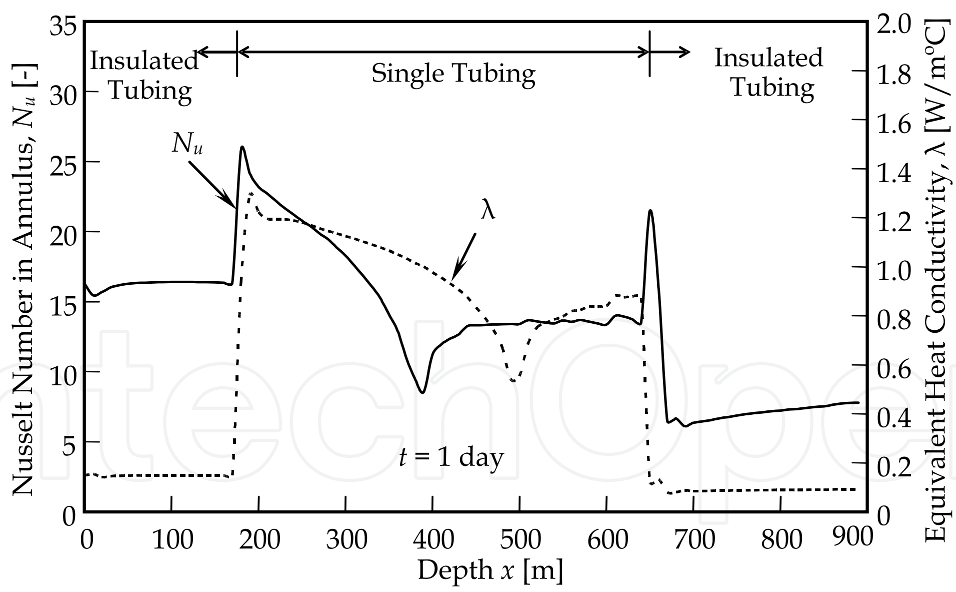

Fig. 17. Nusselt number of convective heat transfer in the annulus vs. depth (Model 2006).

The temperature was still lower than the supercritical temperature (=31.4°C) at the bottom hole because liquid CO_2 filled the annulus and cold CO_2 flow was maintained from 650 to 890m for the insulated tubing despite the formation temperature increasing with depth. The line in Fig. 9 shows s typical phase changes in the injection tubing on the CO_2 pressure-specific enthalpy diagram.

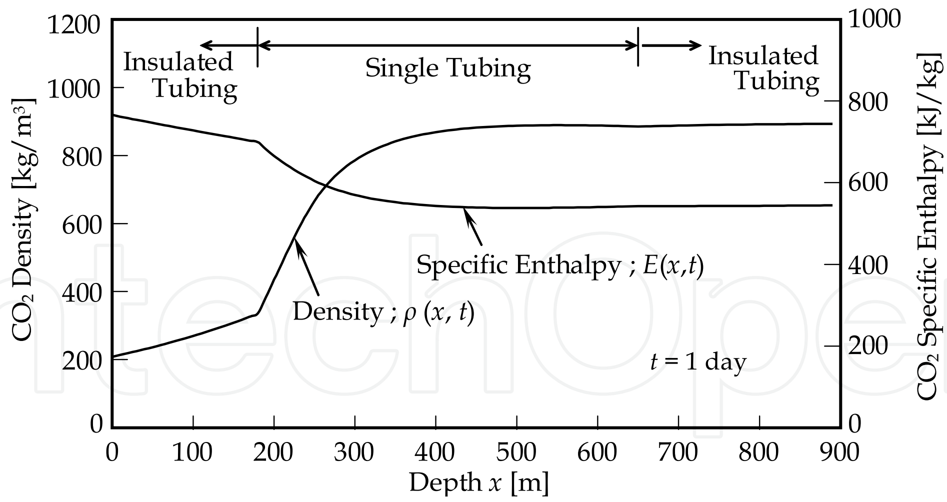

Fig. 18. CO_2 density and specific enthalpy vs. depth (Model 2006).

3.4 All usage of thermal insulated tubing (Model 2007)

In 2007, the all injection tubing pipe was replaced with thermally insulated tubing of 890 m in length and the annulus was filled with water. Figure 13 shows numerical calculation results for Model 2007. The predicted temperature for the bottom hole at an injection rate of 3.0ton/day is 26.0°C, which is lower than the observed temperature at the outer surface of the annulus of 27.5°C. This was influenced by the formation temperature in the annulus.

3.5 The effect of injection rate on the bottom hole temperature

It was expected that the temperature of CO_2 at the bottom hole would increase as the injection rate was increased, since heat loss is not sensitive to flow rate. Figure 19 shows a sensitivity analysis for temperature versus the injection rate at the bottom hole for Model 2007. The CO_2 phase was supercritical at the bottom hole after 1 day when the injection rate was over 12ton/day as shown in this figure. An operation like a hydraulic fracture is required to improve permeability, since the injection rate depends on the permeability around the injection well.

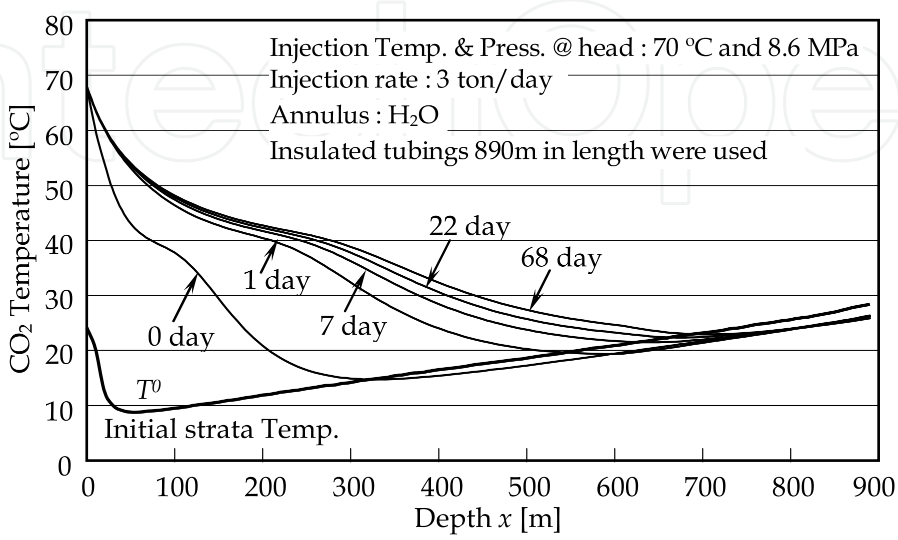

Fig. 19. CO_2 temperature distribution vs. depth for H=H1 (Model 2007)

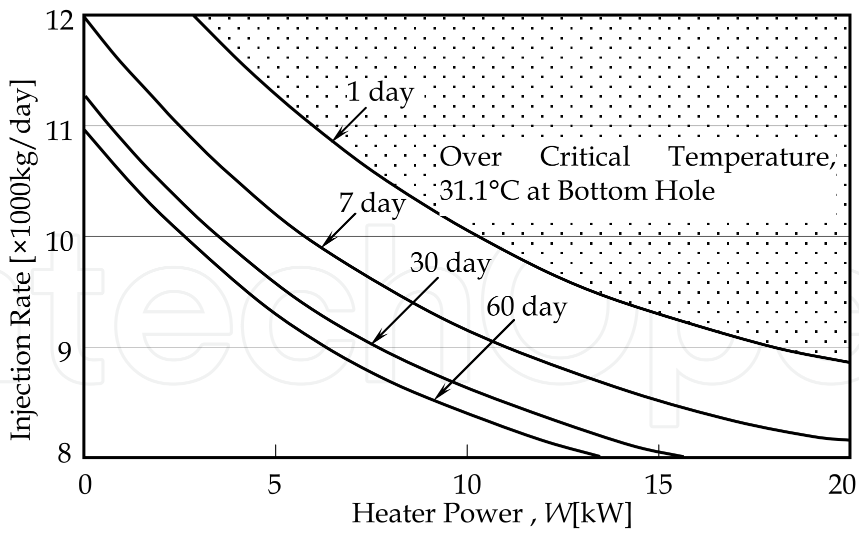

Fig. 20. Control map for maintaining the supercritical condition at the bottom hole (Model 2007+Heater, Injection temperature and pressure at well head; 70 ºC and 8.6 MPa, Annulus; H_2O, Insulated tubing 890m in length was used)

3.6 Prediction of CO_2 temperature using a line heater

All tubing was replaced with thermally insulated tubing but the bottom hole temperature was still not adequate to maintain CO_2 in its critical condition. To overcome the difficulty of injection, numerical predictions were done considering the use of an electric line heater with 1.43kW of heating from the surface to 180m (denoted as Heater Model 2007). The heater capacity of 1.43kW was chosen because of the cable strength and because of restrictions of materials for supercritical CO_2. Table 1 shows conditions used in the calculation. The temperature at the bottom hole from Heater Model 2007 is 5°C higher than that from Model 2007. Even if the energy efficiency of CO_2 injection becomes lower by heating in the injector, it is better that CO_2 temperature is in a supercritical condition at the bottom hole to keep larger CO_2 injection rate into the coal seam. Figure 15 shows a control map for the CO_2 injection rate to maintain the supercritical condition at the bottom. This model shows that the critical temperature increases with the heater power and the elapsed time from the start of CO_2 injection.

4. Summary

In this chapter, a numerical model of heat transfer and calculation procedure for flow and heat transfer phenomena, related to CO_2 flow in a vertical deep injector, has been focused in order to predict CO_2 temperature, pressure and phase change (supercritical or liquid CO_2) in the well. Especially, it was considered that the heat loss from the injector to surrounding casing pipes and rock formation including natural convection heat transfer in annulus and insulated tubing pipes. Furthermore, numerical simulations have been presented for the Yubari CO_2-ECBMR test project carried out from 2005 to 2007.

The results are summarized as follows:

1. The bottom hole pressure and temperature in the injector at Yubari CO_2-ECBMR test field were successfully simulated by considering heat loss accelerated by natural convection flow in the annulus.

2. The thermal equivalent conductivity of the insulated tubing was determined to be 0.21W/m°C based on the well logging temperature carried out at the Yubari test site.
3. A control map showing targeted injection rates against the heater power for elapsed time as a parameter was compiled to maintain the supercritical condition at the bottom hole of the injectior.
4. CO_2 at the bottom hole is expected to be supercritical at a CO_2 injection rate over 12 ton/day without any heating or 11 ton/day using the 1.43kW line heater in the injector.

5. Acknowledgment

Authors would like to express their gratitude to Mr. Tetsu Yasunami, who was a graduate student, Kyushu University for his efforts on numerical simulations. We also thank his kind discussion to Mr. Ferian Angara, who is a PhD student, Kyushu University.

6. Nomenclature

a_f = heat diffusivity of fluid [m²/s]
a_r = heat diffusivity of rock [m²/s]
A = aspect ratio [-]
B_i = Biot number [-]
C_p = isobaric specific heat [kJ/(kg°C)]
E = specific enthalpy [kJ/kg]
E_{WH} = specific enthalpy at well head (x=0) [kJ/kg]
f = friction factor of tubing pipe [-]
g = acceleration of gravity [m/s²]
h_c = circulation height of natural convection flow [m]
h_R = reservoir height [m]
K_w = permeability of reservoir [m²]
L = width of annulus [m]
m = constant number defined by Choukairy et al. (2004) [-]
M = CO_2 mass flow rate [kg/s]
n = correction to adjust heat conductivity in thermally insulated tubing [-]
N_u = Nusselt number [-]
P_{BH} = pressure at bottom hole [MPa]
P_R = pressure at reservoir outer boundary [MPa]
P_r = Prandtl number (=v_f/a_f) [-]
P_{WH} = pressure at well head (x=0) [MPa]
Q = CO_2 flow rate [m³/s]
r_{cao} = outer radius of casing [m]
r_{cai} = internal radius of casing [m]
r_{tuo} = outer radius of single tubing [m]
r_{tui} = internal radius of single tubing [m]
r_{thco} = outer radius of outer thermal insulated tubing [m]
r_{thci} = internal radius of outer thermal insulated tubing [m]
r_{tho} = outer radius of inner thermal insulated tubing [m]
r_{thi} = internal radius of inner thermal insulated tubing [m]
R_a = Rayleigh number [-]

T^0 = initial strata temperature [°C]
T^{an} = temperature of fluid in the annulus [°C]
T_{BH} = temperature at bottom hole [°C]
T^f = CO_2 temperature in tubing [°C]
T_m = dimensionless temperature [-]
T^w = temperature at outer surface of casing [°C]
T_{WH} = temperature at well head (x=0) [°C]
v = average velocity of CO_2 flow in tubing pipe [m/s]
V = specific volume [m³/kg]
x = length from surface (depth) [m]
α_f = heat transfer rate at inner surface of casing [W/(m²°C)]
α_{thi} = heat transfer rate at inner surface of tubing [W/(m²°C)]
α_{ca} = equivalent heat transfer rate at inner casing [W/(m²°C)]
β = coefficient of thermal expansion of CO_2 [1/K]
β_T = coefficient of thermal expansion of the fluid [1/K]
η_t = elapsed time factor [-]
κ = radius ratio [-]
λ = overall heat conductivity [W/(m°C)]
λ_{Ar} = heat conductivity of fluid (Ar) in thermal insulated tubing [W/(m°C)]
λ_f = heat conductivity of fluid (N_2, CO_2 or water) in annulus [W/(m°C)]
λ_r = heat conductivity of rock [W/(m°C)]
λ_{Steal} = heat conductivity of casing and tubing [W/(m°C)]
μ_f = CO_2 viscosity [Pas]
μ_w = water viscosity [Pas]
υ_f = dynamic viscosity [m²/s]
τ = Fourier number [-]
Δq = heat flow rate at tubing element [W]
ΔW = heat generated by a heater during x_i to x_{i+1} [W]
Δx = length of tubing element [m]

7. References

Clarkson, C.R., Pan, Z., Palmer, I. & Harpalani, S. (2008). Predicting Sorption-Induced Strain and Permeability Increase With Depletion for CBM Reservoirs, *Proceedings of SPE Annual Technical Conference and Exhibition* (August, 2008), SPE114778-MS, DOI 10.2118/114778-MS, Society of Petroleum Engineers

Choukairy, K., Eennacer, R. & Vasseur, P. (2004) , Natural Convection in a Vertical Annulus Boarded By An Inner Wall of Finite Thickness, *International Communications in Heat and Mass Transfer*, Vol. 31, pp.501-512, ISSN 0735-1933

Fujioka, M., Yamaguchi, S. & Nako, M. (2010). CO_2-ECBM field tests in the Ishikari Coal Basin of Japan, *International Journal of Coal Geology*, Volume 82, Issues 3-4, 1 June 2010, pp. 287-298, ISSN 0166-5162

Rohsenow, W., Hartnett, J. & Cho, Y. (1998). *An Introduction to Heat Transfer* (May 1998), McGraw-Hill Professional, ISBN-10 0070535558

Michael, A. M., Khepar, S. D. & Sondhi, S. K. (2008). *Water Wells and Pumps*, Tata McGraw-Hill, ISBN(13) 978-0-07-065706-9, New Delhi

Nag, P.K. (2006). *Heat And Mass Transfer.* Tata McGraw-Hill, ISBN 9780070606531, New Delhi

National Institute Standard Technology (NIST) (2010). *Thermophysical Properties of Fluid Systems*, http://webbook.nist.gov/chemistry/fluid/

Sasaki, K. & Akibayashi, S. (1999), A Calculation Model for Liquid CO_2 Injection into Shallow Sub-seabed Aquifer, *Annals of New York Academy of Sciences*, Vol. 912, 1999, pp.211-225, ISSN1749-6632

Sasaki, K. & Dindiwe, C. (2002). Integrated mine ventilation simulator "MIVENA Ver.6" and its applications, *Proceedings of North American/Ninth U.S. Mine Ventilation Symposium*, pp. 243-251, ISBN 9789058093875, CRC Press, Kingston, Canada, June 8-12, 2002

Sasaki, K., Yasunami, T. & Sugai, Y. (2009). Prediction model of Bottom Hole Temperature and Pressure at Deep Injector for CO_2 Sequestration to Recover Injection Rate, *Energy Procedia*, Volume 1, Issue 1 (February 2009), pp. 2999-3006, ISSN 1876-6102

Starfield, A.M. & Bleloch, A.L. (1983). A new Method for The Computation of Heat and Moisture Transfer in a partly Wet Airway, *Journal of South African Institute of Mining and Metallurgy*, Vol. 83, pp.263-269 (November/December, 1983), ISSN 0038-223X

Propath Group (2008). *Manual of PROPATH Version 13.1* (April, 2008), ISSN 0911-1743

Prensky, S. (1992). Temperature Measurements in Boreholes-An Overview of Engineering and Scientific Applications, *The log analyst : a journal of formation evaluation and reservoir description*, Vol. 33-3, pp.313-333, ISSN 0024-581X

Yamaguchi, S., Oga, K., Fujioka, M. & Nako, M. (2007). History Matching on Micro-Pilot Test of CO_2 Sequestration and ECBMR in the Ishikari Coal Field (Coalbed methane(CBM), *Journal of the Japan Institute of Energy*, Vol. 86-2, 2007, pp.80-86, ISSN 0916-8753

Yasunami, T., Sasaki, K. & Sugai, Y. (2010). CO_2 Temperature Prediction System in Injection Tubing Considering Supercritical Condition at Yubari ECBM Pilot-Test, *Journal of Canadian Petroleum Technology (Society of Petroleum Engineers)*, Vol. 49-4 (April, 2010), pp. 44-50, ISSN 00219487

Yee, D., Seidle, J.P. & Hanson, W.B. (1993). Gas Sorption on Coal and Measurement of Gases content, *AAPG Studies in Geology*, Vol. 38 (May, 1983), pp. 203-218, ISSN 0 89181-049-8

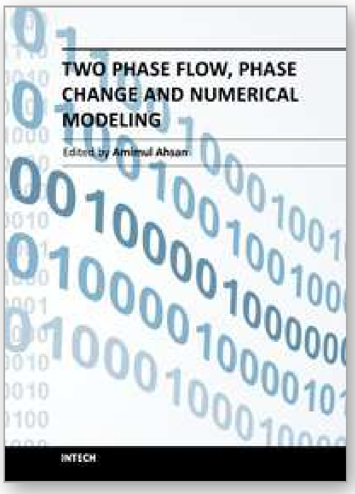

Two Phase Flow, Phase Change and Numerical Modeling
Edited by Dr. Amimul Ahsan

ISBN 978-953-307-584-6
Hard cover, 584 pages
Publisher InTech
Published online 26, September, 2011
Published in print edition September, 2011

The heat transfer and analysis on laser beam, evaporator coils, shell-and-tube condenser, two phase flow, nanofluids, complex fluids, and on phase change are significant issues in a design of wide range of industrial processes and devices. This book includes 25 advanced and revised contributions, and it covers mainly (1) numerical modeling of heat transfer, (2) two phase flow, (3) nanofluids, and (4) phase change. The first section introduces numerical modeling of heat transfer on particles in binary gas-solid fluidization bed, solidification phenomena, thermal approaches to laser damage, and temperature and velocity distribution. The second section covers density wave instability phenomena, gas and spray-water quenching, spray cooling, wettability effect, liquid film thickness, and thermosyphon loop. The third section includes nanofluids for heat transfer, nanofluids in minichannels, potential and engineering strategies on nanofluids, and heat transfer at nanoscale. The forth section presents time-dependent melting and deformation processes of phase change material (PCM), thermal energy storage tanks using PCM, phase change in deep CO2 injector, and thermal storage device of solar hot water system. The advanced idea and information described here will be fruitful for the readers to find a sustainable solution in an industrialized society.